Journal of Chemical Crystallography (2022) 52:324–336
https://doi.org/10.1007/s10870-022-00930-8

ORIGINAL PAPER

Crystal Structure Characterization, Hirshfeld Surface Analysis, and Non-covalent Interactions of 2,5-Bis(4-chlorophenyl)-1,3,4-Oxadiazole

P. Akhileshwari[1] · K. Sharanya[2] · M. A. Sridhar[1]

Received: 23 December 2021 / Accepted: 10 February 2022 / Published online: 2 March 2022

Abstract

Heterocyclic compounds are present abundantly in nature. Nitrogen containing heterocyclic compounds are an important class which made significant contributions to medicinal chemistry. Oxadiazole derivatives are scaffolds which exhibit wide range of biological applications. The title compound was synthesized and crystallizes in the orthorhombic crystal system. The structure exhibits C–H…N intermolecular interactions. The structure is stabilized by π–π interactions between the oxadiazole and phenyl rings. Intermolecular interactions are quantified by Hirshfeld surface analysis. Energy frameworks are constructed to investigate the stability of the compound. Molecular geometry calculations are performed using density functional theory by employing 6–31 + G (d, p) functional basis set. The chemical significant sites are identified by topology analysis.

Graphical Abstract

The research article presents the synthesis of 2,5-bis(4-chlorophenyl)-1,3,4-oxadiazole, and single crystal XRD study to unveil the crystal parameters. Intermolecular interactions were explored by Hirshfeld surface analysis. Further, computational analysis were performed.

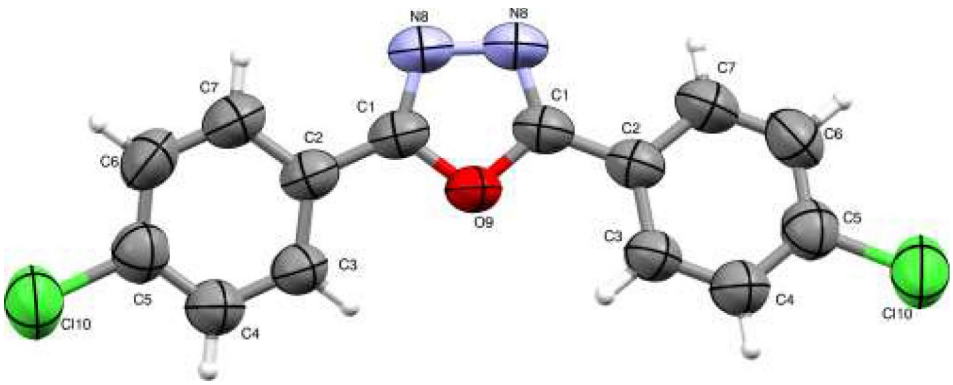

ORTEP of the molecule with thermal ellipsoids drawn at 50% probability

Keywords Oxadiazole · XRD · Hirshfeld surface analysis · Energy frameworks · HOMO–LUMO

✉ M. A. Sridhar
mas@physics.uni-mysore.ac.in

Extended author information available on the last page of the article

Introduction

Heterocycles are inextricably woven into our life processes. Numerous molecules having heteroatoms such as nitrogen, oxygen, and sulfur have drawn the interest of researchers in pharmaceutical and agrochemical industries [1]. The multiple pharmacological actions of heterocyclic compounds are a prerequisite for classifying a drug as highly efficacious, because these actions offer the possibility of treating various diseases [2]. These compounds possess the ability to interact with various biomolecules in multiple ways, such as hydrogen bonding, π stacking interactions, van der Waals interactions, metal coordination bonds, and hydrophobic forces etc. [3]. A large number of natural and synthetic heterocyclic compounds are known for their therapeutic values. With their diverse structure and functional versatility, the heterocyclic compounds will continue to play a very important role in the construction of lead compounds in drug discovery.

One of the extensively studied azole based heterocyclic compounds is oxadiazole derivative. This is a commonly used pharmacophore due to its ability to engage in hydrogen-bonding, metabolic stability and favourable ADME properties [4, 5]. Oxadiazoles are also known as bioisoesters for amide, ester, ketone, carbamate functionalities [6, 7]. During the past years, considerable evidences have been found for their broad spectrum of biological activity, including antimicrobial [8], analgesic [9], antiinflammatory [10], anticancer [11], anticonvulsant [12], monoamine oxidase inhibitors [13], and tyrosinase inhibitors [14]. 1,3,4-Oxadiazole-carboxamides containing different lipophilic moieties (i.e., 4-diphenyl, 1-napthyl, phenyl propyl and *n*-hexyl substituents) and additional substituents, such as alkyl and amino alkyl residues, have been described as antiplatelet, antithrombotic and serotonin antagonist [15]. 2-Amino-1,3,4-oxadiazole has been proven to be a muscle relaxant [16]. Oxadiazole nucleus is present in several marketed drugs, such as raltegravir (anti-HIV), Zibotentan (anticancer), Nesapidil (anti-arrhythmic), Tiodazosin (antihypertensive) etc. [17].

Oxadiazole exhibits four isomers such as 1,2,5-oxadiazole, 1,2,4-oxadiazole, 1,3,4-oxadiazole and 1,2,3-oxadiazole. Among these, 1,3,4-oxadiazoles have shown great utility in pharmaceutical industry during the past years. In order to synthesize 1,3,4-oxadiazoles, several methods are available in the literature. The most common synthetic route used for 1,3,4-oxadiazole includes reactions of acid chlorides/carboxylic acids with acid hydrazides (or hydrazine) and direct cyclization of diacylhydrazines using dehydrating agents. The commonly used dehydrating agents are phosphorous oxychloride, triflic anhydride, thionyl chloride, phosphorous pentaoxide, polyphosphoric acid, and direct reaction of acid with (N-isocyanimino-) triphenylphosphorane etc. [18]. In this study, we present the synthesis of 2,5-bis(4-chlorophenyl)-1,3,4-oxadiazole, and single crystal XRD study to unveil the crystal parameters. Intermolecular interactions were explored by Hirshfeld surface analysis. Further, computational analysis were performed.

Materials and Methods

All chemical reagents were purchased from commercial suppliers and used without further purification. The reactions were monitored by thin layer chromatography (TLC) using pre-coated sheets of silica gel (Merck 60F254, 0.25 mm thickness) and visualized under UV light.

Synthesis of 2,5-Bis(4-chlorophenyl)-1,3,4-Oxadiazole

An equimolar mixture of 4-chlorobenzhydrazide and 4-chlorobenzoic acid was refluxed in the presence of phosphorous oxychloride for 6 h. The reaction mixture was cooled and poured into the crushed ice [19–21]. On neutralization with a solution of sodium bicarbonate, a solid mass was formed. The product was separated out, filtered, washed, and dried. It was recrystallized using ethanol by the slow evaporation method. The synthetic procedure for the title molecule is depicted in Fig. 1.

Experimental

Single Crystal X-ray Diffraction

A small block of crystal was selected for the single crystal X-ray diffraction study. The intensity data were collected at

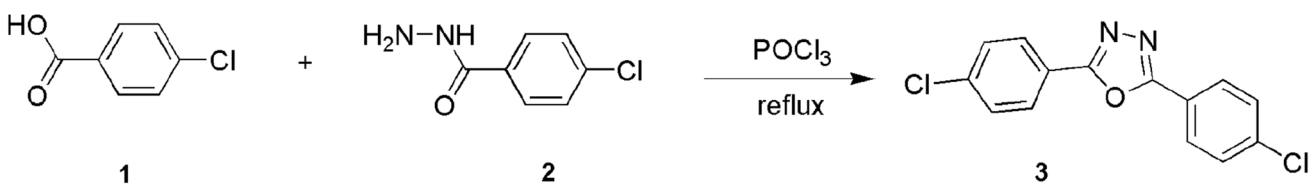

Fig. 1 Reaction scheme for the synthesis of the title molecule

the room temperature of 293 (2) K on Bruker Venture diffractometer using Cu*Kα* radiation. The data sets were processed using *SADABS* software. The structure was solved by direct methods and refined by full-matrix least squares methods on F^2 using *SHELXS* and *SHELXL* [22] programs respectively. All non-hydrogen atoms of the molecule are revealed by E-map drawn by the correct set of phases. All carbon bound hydrogen atoms were positioned geometrically and refined using a riding model with C–H = 0.93 Å with U_{iso} (H) = 1.2U_{eq}(C). The geometrical calculations were performed using *PLATON* program [23]. *ORTEP* of the molecule with thermal ellipsoids and packing diagrams were generated using *Mercury* [24] software. A total of 88 parameters were refined with 1317 unique reflections out of 14,393 of observed reflections. After several cycles, the residual value R saturated to 0.0519 with a goodness of fit 1.130. A summary of crystal data and refinement details are listed in Table 1. The values of bond lengths, bond angles, and torsion angles are tabulated in the Tables 2, 3, and 4 respectively.

Table 1 Crystal data and refinement parameters of the molecule

Empirical formula	C_{14} H_8 CL_2 N_2 O
Formula weight	291.12
Temperature	296 (2) K
Wavelength	1.54178 Å
Crystal system	Orthorhombic
Space group	*Pbcn*
Cell dimensions	a = 5.1040 (6) Å, b = 12.5238 (13) Å, c = 20.726 (2) Å
Volume	1324.8 (2) $Å^{-3}$
Z	4
Density (calculated)	1.460 Mg m^{-3}
Absorption coefficient	4.346 mm^{-1}
F_{000}	592
Crystal size	0.20 mm × 0.25 mm × 0.30 mm
θ range for data collection	4.27° to 72.75°
Index ranges	$-6 \le h \le 5$ $-15 \le k \le 14$ $-25 \le l \le 25$
Reflections collected	14,393
Independent reflections	1317 [R_{int} = 0.058]
Refinement method	Full matrix least-squares on F^2
Data/restraints/parameters	1317/0/88
Goodness-of-fit on F^2	1.130
Final [I > 2σ(I)]	*R*1 = 0.0519, *wR*2 = 0.1582
R indices (all data)	*R*1 = 0.0586, *wR*2 = 0.1693
Extinction coefficient	0.013 (3)
Largest diff. peak and hole	0.291 and − 0.250 *e* $Å^{-3}$

Table 2 Bond lengths of the non hydrogen atoms

Atoms	Length (Å)		Atoms	Length (Å)	
	XRD	DFT		XRD	DFT
CL10–C5	1.737 (3)	1.720	C2–C7	1.389 (3)	1.404
O9–C1	1.362 (2)	1.371	C3–C4	1.366 (3)	1.399
N8–C1	1.293 (3)	1.317	C4–C5	1.377 (4)	1.393
N8–N8	1.397 (3)	1.379	C5–C6	1.379 (4)	1.392
C1–C2	1.450 (3)	1.457	C6–C7	1.372 (4)	1.398
C2–C3	1.391 (3)	1.404			

Results and Discussion

Crystal Structure Analysis

The molecule crystallizes in the orthorhombic crystal system with the space group *Pbcn*. The asymmetric unit contains half of the molecule (Z′ = 0.5). The unit cell parameters are: a = 5.1040 (6) Å, b = 12.5238 (13) Å, c = 20.726 (2) Å. The *ORTEP* of the molecule is shown in Fig. 2.

The crystal structure consists of oxadiazole ring and chlorophenyl ring. The bond length of N8–N8 atoms in oxadiazole ring is 1.397 (3) Å, which is similar to the bond length of typical a N–N contact. The observed bond lengths of N8–C1 and CL10–C5 atoms are 1.293 (3)°, and 1.737 (3)° respectively, which are consistent with the standard bond lengths [25]. In oxadiazole ring, the bond angle of the N8–C1–O9 atoms is 111.8 (2)°. The torsion angle of C3–C2–C7–C6 atoms is 0.2 (4)°, indicating the + *syn*-periplanar conformation. The phenyl ring is sp^2 hybridized and shows trigonal geometry as indicated by the bond angles between the atoms C2–C3–C7 = 120.2 (2)°, C1–C2–C7 = 120.7 (2)°, C2–C3–C4 = 119.4 (5)°, C3–C4–C5 = 119.2 (2)°, C4–C5–C6 = 121.0 (2)°, C5–C6–C7 = 119.6 (2)°, C2–C7–C6 = 120.2 (2)°. The chlorophenyl ring C2 to C7 is highly planar with a maximum r.m.s. deviation of 0.001 (2) Å for the C7 atom. The

Table 3 Bond angles of the non hydrogen atoms

Atoms	Angle (°)		Atoms	Angle (°)	
	XRD	DFT		XRD	DFT
C1–O9–C1	103.3 (2)	117.5	C2–C3–C4	120.7 (2)	120.7
N8–N8–C1	106.6 (2)	106.5	C3–C4–C5	119.4 (2)	119.8
O9–C1–N8	111.8 (2)	112.5	CL10–C5–C4	118.8 (2)	119.8
O9–C1–C2	119.1 (2)	117.5	CL10–C5–C6	120.3 (2)	119.8
N8–C1–C2	129.1 (2)	129.9	C4–C5–C6	121.0 (2)	120.3
C1–C2–C3	120.6 (2)	121.9	C5–C6–C7	119.6 (2)	119.7
C1–C2–C7	120.2 (2)	119.6	C2–C7–C6	120.2 (2)	120.8
C3–C2–C7	119.2 (2)	118.4			

Table 4 Torsion angles of the non hydrogen atoms

Atoms	Angle (°)		Atoms	Angle (°)	
	XRD	DFT		XRD	DFT
C1–O9–C1–N8	0.3 (2)	0.00	C7–C2–C3–C4	0.8 (3)	0.0
C1–O9–C1–C2	179.1 (2)	− 180.0	C1–C2–C7–C6	179.8 (2)	− 180.0
C1–N8–N8–C1	1.0 (3)	− 0.00	C3–C2–C7–C6	− 0.2 (4)	0.00
N8–N8–C1–O9	− 0.8 (3)	0.00	C2–C3–C4–C5	− 0.7 (4)	− 0.0
N8–N8–C1–C2	− 179.4 (2)	− 180.0	C3–C4–C5–CL10	− 180.0 (2)	180.0
O9–C1–C2–C3	− 7.8 (3)	− 0.0	C3–C4–C5–C6	− 0.2 (4)	0.00
O9–C1–C2–C7	172.2 (2)	179.9	CL10–C5–C6–C7	− 179.4 (2)	− 180.0
N8–C1–C2–C3	170.7 (2)	179.9	C4–C5–C6–C7	0.8 (4)	− 0.0
N8–C1–C2–C7	− 9.3 (4)	− 0.01	C5–C6–C7–C2	− 0.6 (4)	0.01
C1–C2–C3–C4	− 179.2 (2)	180.0			

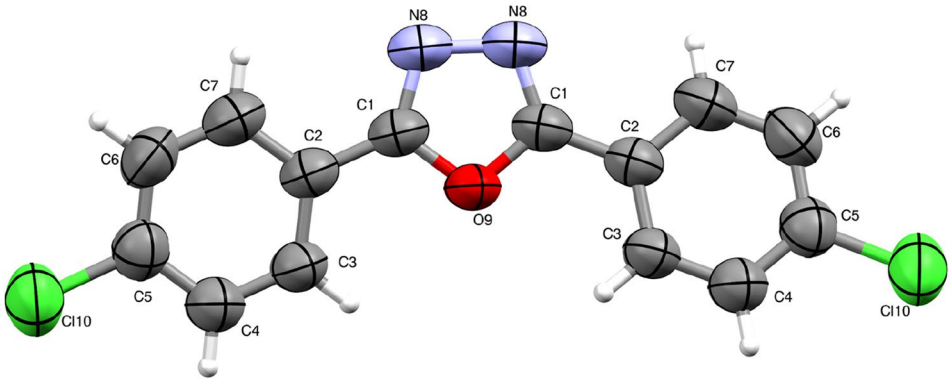

Fig. 2 *ORTEP* of the molecule with thermal ellipsoids drawn at 50% probability.

Table 5 Hydrogen bond geometry

D–H…A	D–H (Å)	H…A (Å)	D…A (Å)	D–H…A (°)
C3–H3…N8[a]	0.93	2.66	3.326 (3)	129
C3–H3…O9*	0.93	2.50	2.826 (2)	100

*Intra

[a]1/2 − *x*, 1/2 + *y*, *z*

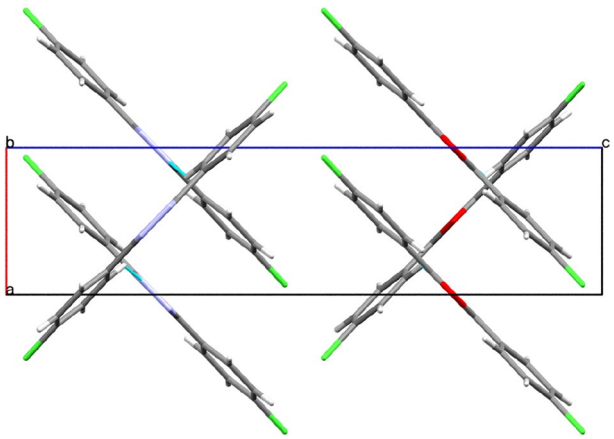

Fig. 3 Packing of molecules showing criss-cross orientation when viewed along *b* axis

oxadiazole ring is nearly planar with a maximum deviation of 0.003 (2) Å for the C1 atom. The torsion angle between the C1–C2–C7–C6 and C3–C4–C5–CL10 atoms is 179.8 (2)° and − 180.0 (2)° respectively. The crystal structure is reinforced by C–H…N intermolecular interaction and C–H…O intramolecular interactions. Hydrogen bond geometry is shown in Table 5. Packing of molecules shows a criss-cross orientation when viewed along *b* axis (Fig. 3).

Supramolecular Assembly

The presence of C–H…π interaction and π–π interactions in the crystal structure consolidate the supramolecular architecture. The molecule exhibits C5–CL10…π (Cg2) interaction. Cg2 is the centroid of the phenyl ring (C2–C3–C4–C5–C6–C7). The C5–Cg distance is 3.782 (14) Å, C5–CL10…Cg angle is 95.14 (9)°, γ = 14.5°, and CL–Cg = 4.301 (3) Å, with the symmetry code 1 + *x*, *y*, *z*. The structure is stabilized by medium to weak π–π interaction as the Cg–Cg distance is 3.8058 (14) Å, with α = 8.52 (12)°, β = 21.8°, γ = 13.8°, and a slippage value 1.412° [26]. The symmetry code for the interaction is − 1 + *x*, *y*, *z*. The π–π interaction of molecules involving phenyl ring and oxadiazole ring is shown in Fig. 4.

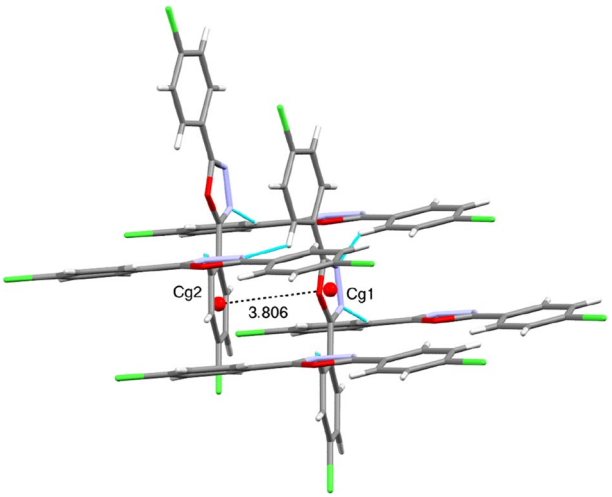

Fig. 4 π–π interaction of molecules involving phenyl ring and oxadiazole ring

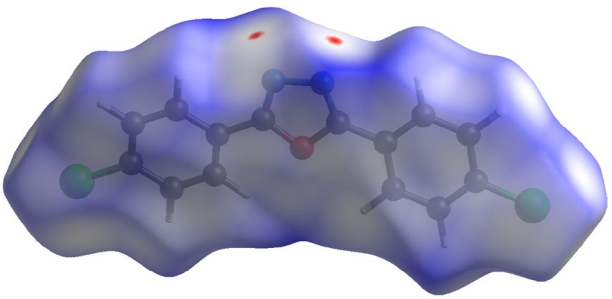

Fig. 5 Hirshfeld surface of the molecule mapped with d_{norm}

Hirshfeld Surface Analysis

Hirshfeld surface analysis is a tool used to visualize the intermolecular interaction in the crystal system. Two dimensional fingerprint plots give the summary of intermolecular contacts in the crystal. The Hirshfeld surfaces and fingerprint plots are generated using *CrystalExplorer17.5* [27]. The Hirshfeld surface analysis confirms the presence of the C–H…N intermolecular contact, which influences the molecular packing. Molecular Hirshfeld surface of the crystal structure is constructed on the basis of electron distribution, calculated as the sum of spherical atom electron densities [28]. The normalized contact distance (d_{norm}) is given by,

$$d_{\text{norm}} = \frac{d_i - r_i^{vdw}}{r_i^{vdw}} + \frac{d_e - r_e^{vdw}}{r_e^{vdw}},$$

where d_e is the distance from the surface to the nearest nucleus in another molecule; d_i is the distance internal to the surface (i.e., distance from the surface to the nearest atom in the molecule itself). The value of d_{norm} is dependent on the contacts which are shorter and longer than the van der Waals radii (r^{vdw}).

From Fig. 5, the red and blue colors on the Hirshfeld surface indicate distances shorter (close contact) or longer (distinct contact) than the van der Waals radii respectively, and the white region indicates contacts with distances equal to the sum of van der Waals radii. The bright red spots on the Hirshfeld surface are due to the presence of the C–H…N intermolecular interactions.

Figure 6 depicts the Hirshfeld surface mapped with (a) curvedness map, (b) shape index map, and (c) electrostatic potential map of the title molecule. The bright red spots on the electrostatic potential map indicate the donors and/or acceptors. The red region indicates the negative electrostatic potential (hydrogen bond donors), while the blue region indicates positive electrostatic potential (hydrogen bond acceptors). The shape index map of the Hirshfeld surface helps to visualize the π–π stacking arrangement of molecules by the presence of adjacent red and blue triangles [29–36]. If the adjacent red and/or blue triangles are absent, then there are no π–π interactions. In the Fig. 6b, the adjacent red and blue triangles clearly indicate the presence of π–π interactions in the crystal.

Fingerprint Plots

Two dimensional fingerprint plots generated by d_e and d_i provide a concise summary about individual intermolecular interactions [37]. The observed interatomic contacts with their relative contributions to the Hirshfeld surface are H–H (26.5%), Cl–H/H–Cl (19.9%), N–H/H–N (14.3%), and C–H/H–C (11.3%) (Fig. 7). The major contact is H…H

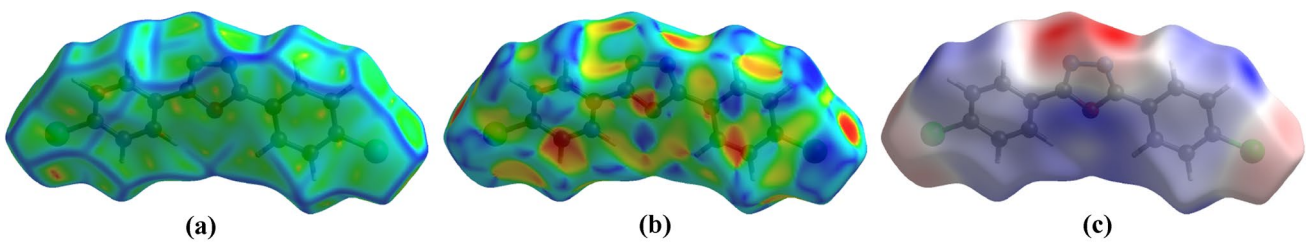

Fig. 6 Hirshfeld surface mapped with **a** curvedness map, **b** shape index map, and **c** electrostatic potential map of the molecule

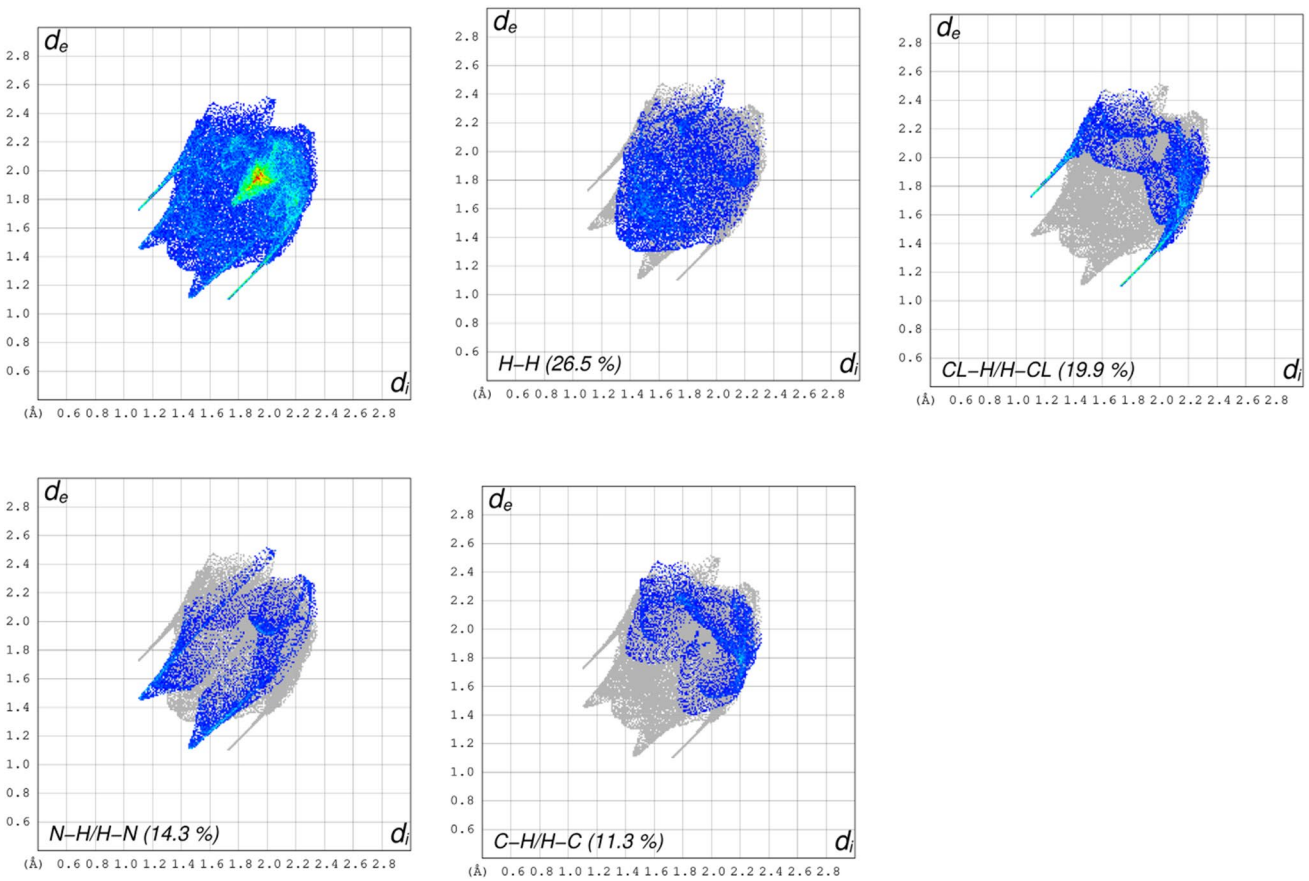

Fig. 7 Fingerprint plots indicating the individual contributions to the Hirshfeld surface area

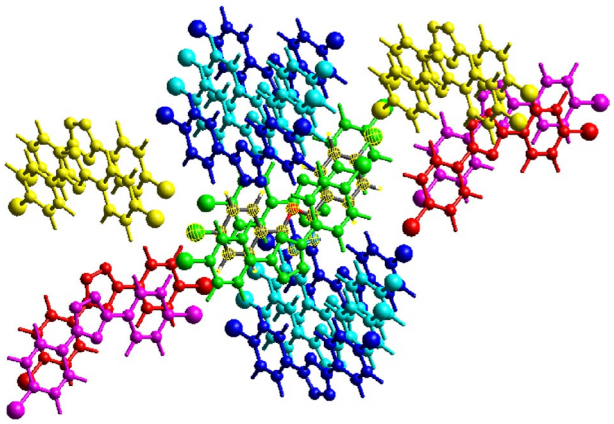

Fig. 8 Molecular pairs involved in the computation of interaction energies

interactions, contributing 26.5% to the overall crystal packing. The pair of spikes in the fingerprint plot delineated into Cl–H/H–Cl contacts, contributes 19.9% with the thin edges at $d_e + d_i \sim 2.8$ Å. The red color in the center of the fingerprint plot indicates the π–π interactions present in the crystal. The N–H/H–N contacts comprise 14.3% of Hirshfeld surface area and is observed as a pair of wings (Fig. 7).

Interaction Energy Analysis

CrystalExplorer17.5 software [27] was employed to compute the intermolecular interaction energies using B3LYP/6-31G (d, p) energy model. A cluster of molecules was generated by importing crystallographic file with a radius of 3.8 Å. The total intermolecular energy (E_{tot}) is defined as the sum of electrostatic (E_{ele}), polarization (E_{pol}), dispersion (E_{dis}) and repulsion (E_{rep}) energies,

$$\text{i.e.,}\ E_{tot} = k_{ele}E_{ele} + k_{po}E_{pol} + k_{dis}E_{dis} + k_{rep}E_{rep},$$

where k_{ele}, k_{po}, k_{dis}, and k_{rep} are the scale factors of 1.057, 0.740, 0.871 and 0.618, respectively [38].

Molecular pairs involved in the computation of interaction energies is shown in Fig. 8. Different interaction energies such as electrostatic energy, dispersion energy, polarization energy and repulsion energy are − 21.668 kJ/mol, − 4.22 kJ/mol, − 90.41 kJ/mol, and 34.35 kJ/mol respectively. The total interaction energy is − 81.2 kJ/mol.

Table 6 Interaction energies (Color table online)

	N	Symop	R	E_ele	E_pol	E_dis	E_rep	E_tot
	2	− x, − y, − z	11.69	− 0.8	− 0.2	− 10.3	2.2	− 8.6
	4	− x+1/2, − y+1/2, z+1/2	11.58	− 1.9	− 0.1	− 6.5	6.6	− 3.7
	2	X, y, z	5.10	− 1.6	− 1.1	− 58.2	23.6	− 38.7
	4	X+1/2, y+1/2, − z+1/2	6.76	− 10.3	− 3.4	− 13.4	11.2	− 18.2
	4	X+1/2, y+1/2, − z+1/2	9.89	− 0.5	− 0.5	− 7.3	2.5	− 5.8
	2	− x, − y, − z	14.65	− 5.4	− 0.4	− 8.1	11.1	− 6.2

The molecular pair-wise interaction energies are listed in Table 6. The dispersion energy dominates the electrostatic energy. The interaction energies are visualized by constructing 3D energy frameworks (Fig. 9). The size of cylinders in the energy frame works reflects the strength of the interaction energy and molecular packing [39].

Hydrogen-bonding interaction energies (kJ/mol) were calculated to be 13.0 (E_{ele}), 1.8 (E_{pol}), 68.0 (E_{dis}), 48.3 (E_{rep}) and 44.4 (E_{tot}) for the C–H…N hydrogen bonding interaction. The hydrogen bond interaction energies for C–H…O contact is 37.3 (E_{ele}), 9.3 (E_{pol}), 19.0 (E_{dis}), 33.7 (E_{rep}) and 42.0 (E_{tot}).

Density Functional Theory (DFT)

Molecular Geometry Optimization

The geometry optimization of the compound was carried out theoretically in the gaseous phase using DFT calculation with B3LYP/6–31 + G (d, p) hybrid functional. The DFT calculations were performed using *Gaussian* software [40]. Theoretically determined structure parameters show good agreement with the results of XRD analysis. The differences between the bond lengths and bond angles are within normal ranges and consistent with the similar types of compounds reported earlier [41]. The comparison of the structure parameters are can be seen in Tables 2, 3, and 4 respectively. An overlay of the experimental structure (pink) and optimized structure (blue) is showing in Fig. 10.

The linear correlation coefficients (R^2) between the theoretical and experimental structure parameters are calculated. The R^2 value for bond length and bond angle are 0.8621 and 0.9935 respectively. Figure 11 gives the agreement between the computed and calculated bond length and bond angle as a linear graph.

Frontier Molecular Orbital

Highest Occupied Molecular Orbital (HOMO) and Lowest Unoccupied Molecular Orbital (LUMO) together are known as frontier molecular orbitals. They are very important parameters in describing the chemical reactivity and kinetic stability of the molecule. HOMO acts as an electron donor, and the LUMO acts as an electron acceptor. A molecule is said to be highly polarizable, if the energy gap is small and has high chemical reactivity. The energy difference between the HOMO and LUMO is the energy gap. The energy level diagram of the HOMO and LUMO is shown in Fig. 12. The HOMO and LUMO are localized over the entire ring of the molecule. The energy gap of the title molecule is found to be 4.30 eV. The energy gap is comparable with the values of similar molecules reported earlier [42]. The value of energy gap indicates the title molecule is kinetically stable and reactive [43].

Chemical reactivity descriptors were derived from the energies of HOMO and LUMO. The energy of HOMO and LUMO are − 6.60 eV and − 2.30 eV respectively. The calculated reactivity descriptors such as ionization potential, electron affinity, chemical hardness, softness, electronegativity, chemical potential and electrophilicity of the title compound are listed in Table 7.

Mulliken Atomic Charge Analysis

Mulliken atomic charges gives us a better understanding to analyze the quantum chemical systems, which intern bearing the properties of dipole moment, electronic structure, and polarizability [44]. Mulliken atomic charges of individual atom of the title compound have been computed using B3LYP functional with 6–31 + G (d, p) level. Mulliken charges for non-hydrogen atoms ranges from 0.0466 to 0.5248. The atoms C7, O8, and CL10 carry high Mulliken charge for the title molecule. The carbon atom C7 (0.524) shows high electropositive value due to the influence of surrounding electronegative C6 (− 0.252) and C2 (− 0.141) atoms, while O8 (− 0.292) has low electronegative value among all other hetero atoms due to electropositive C1 (0.165) atom. The charge distribution of non-hydrogen atoms is shown in Fig. 13.

Molecular Electrostatic Potential (MEP)

Molecular electrostatic potential (MEP) is an implement to predict the electrophilic and nucleophilic attacks for the molecular interactions. The MEP of the title compound was optimized using B3LYP method via 6–31 + G (d, p) basis set. As observed in the Fig. 14, the electrostatic potential is represented as different colored regions on the surface

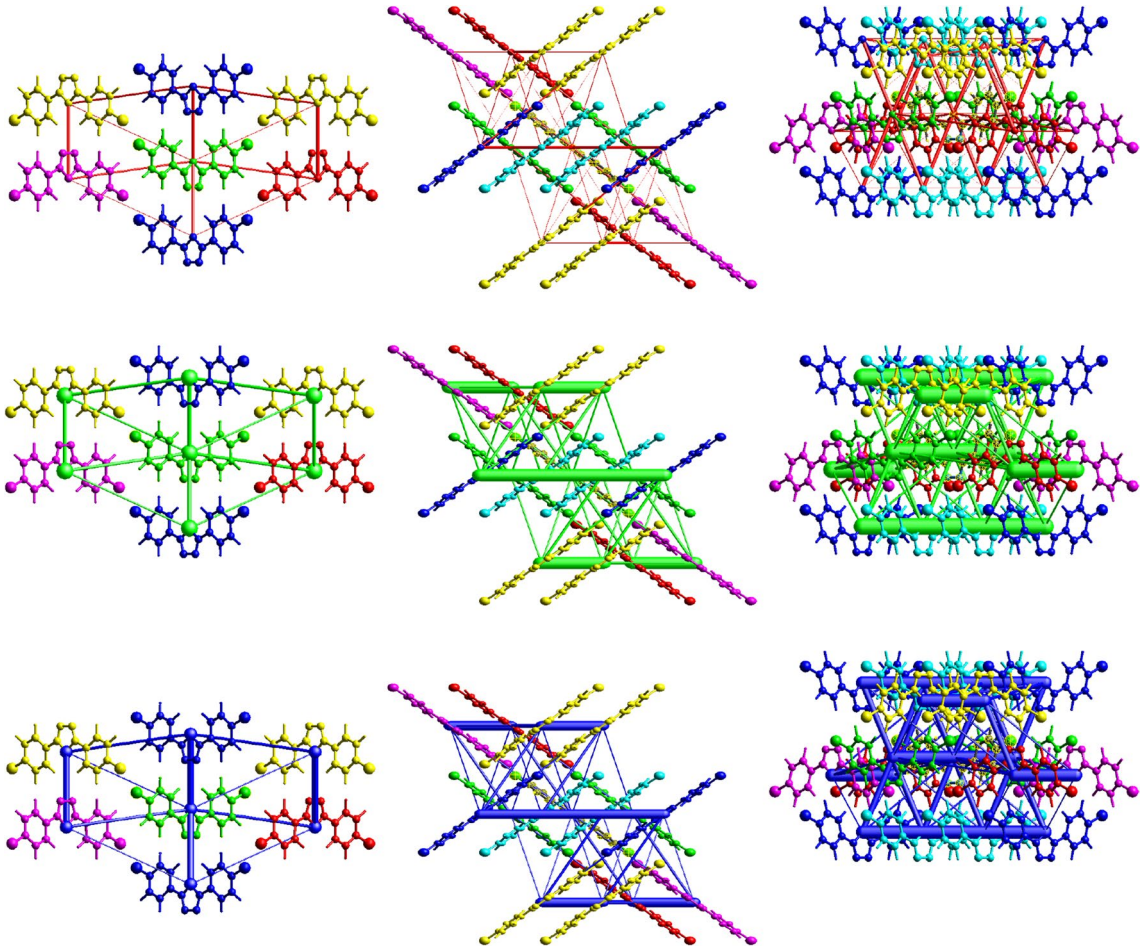

Fig. 9 Molecular packing corresponding to coulomb energy (red), dispersion energy (green), and total energy (blue) along *a*, *b*, and *c* axis respectively (Color figure online)

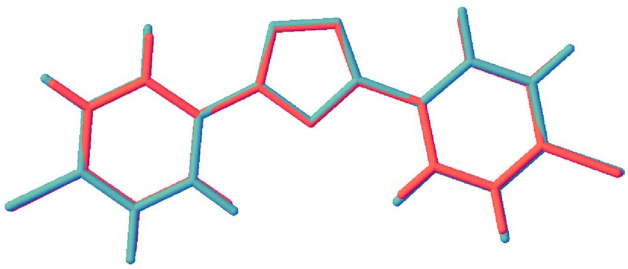

Fig. 10 Overlay of the experimental structure (pink) and optimized structure (blue) (Color figure online)

indicated by red < orange < yellow < green < blue colors. The deep blue regions (positive potential regions) on the molecular surface indicate the electrophilic sites, and the red colored regions indicate the nucleophilic sites. The blue colored regions situated around hydrogen atoms represent a positive potential. The negative potential (repulsion) is indicated by the red colored regions around nitrogen atoms. The region of negative potential is associated with the lone pair of electronegative atoms [45].

Electron Localization Function (ELF) and Local Orbital Localization (LOL)

ELF was widely used in revealing the atomic shell structure, and in the classification of chemical bonding. Electron localization function was proposed by Becke and Edgecombe to determine the regions of electron localization. Savin et al. interpreted the ELF as excess of kinetic energy density caused by Pauli repulsion [46]. A large value of ELF denotes the localization of electrons and indicates the presence of covalent bond. Local orbital localization (LOL) is a function for identifying the high localization regions like ELF [47]. The quantitative values of ELF and LOL are highlighted by

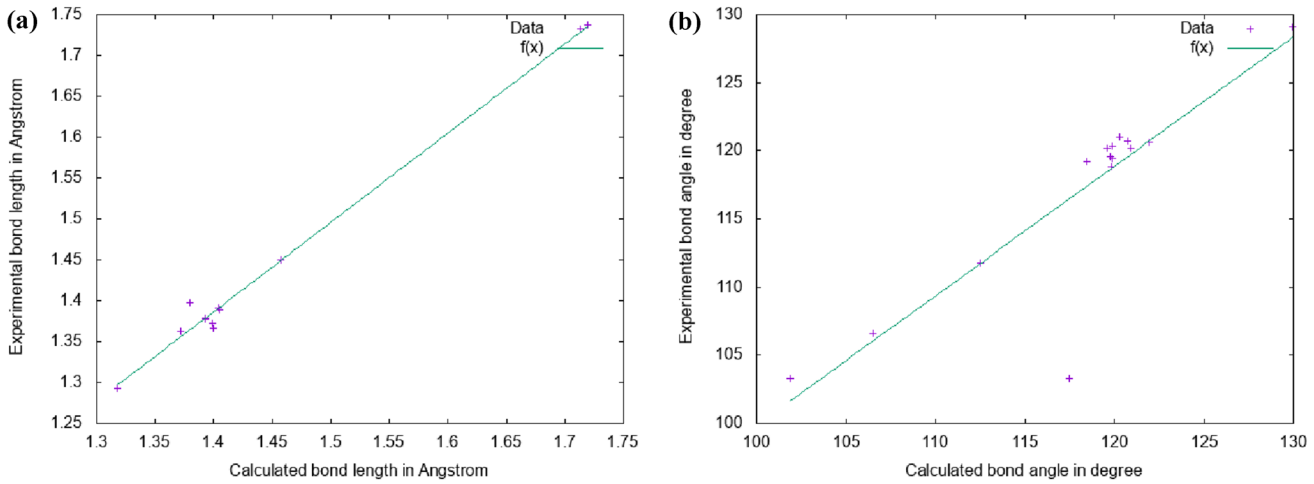

Fig. 11 Correlation graph of **a** bond lengths, and **b** bond angles

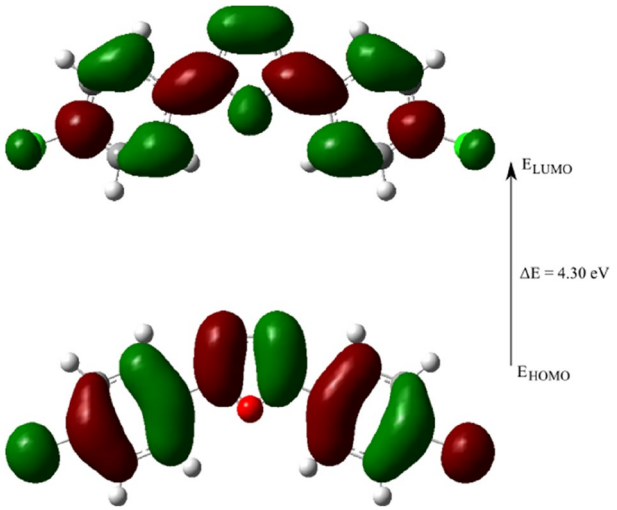

Fig. 12 The energy level of frontier molecular orbital (HOMO–LUMO)

Table 7 Molecular reactivity descriptors and their energies

Parameter	Value (eV)
E_{HOMO}	− 6.60
E_{LUMO}	− 2.30
Energy gap (ΔE)	4.30
Ionization potential (I)	6.60
Electron affinity (E)	2.30
Chemical potential (μ)	− 4.45
Electronegativity (χ)	4.45
chemical hardness (η)	2.15
Global softness (σ)	0.47
Electrophilicity (ω)	4.60

chemically significant regions. LOL can be interpreted in view of the localized orbital.

A small LOL value usually appears in the boundary (inner) region of localized orbitals. The values of LOL and ELF range from 0 to 1. The value greater than 0.5 represent the region of electron localization whereas value less than 0.5 indicate electron delocalization of region. From Fig. 15, it is observed that the red colored regions around the hydrogen atoms represent the high localization nature of bonding and non-bonding atoms, and the blue colored regions represent the delocalization of electrons. The degree of electron localization between N–N bond is not the same as C–C bonds, and C–O bonds (Fig. 14).

Non-covalent Interactions (NCIs)

Non-covalent interactions (NCIs) also known as Reduced Density Dradient (RDG) is a method for studying weak interactions. DFT calculations were performed to analyze the reduced density gradient using *Gaussian* software [40] with B3LYP/6–31 G (d, p) basis set. The pictorial representation of RDG isosurface is obtained using *Multiwfn* [48] and *VMD* software [49]. The RDG isosurface and the graph of RDG against sign(λ_2)ρ(r) is shown in Fig. 16. It reveals the nature and strength of the interactions present in the molecule. The RDG analysis was carried out at the isosurface value of 0.5. The strength of weak interaction has positive correlation with the electron density ρ; the van der Waals interaction regions have very small ρ, while the strong steric effect and hydrogen bonding have relatively large regions corresponding to the electron density ρ [50].

The spikes in the Fig. 16b is classified into three types, namely van der Waals, steric effect, and hydrogen bond interaction. The blue color implies the strong attractive interaction; but hydrogen bond is not interaction observed. The van der Waals weak interaction regions have represented by

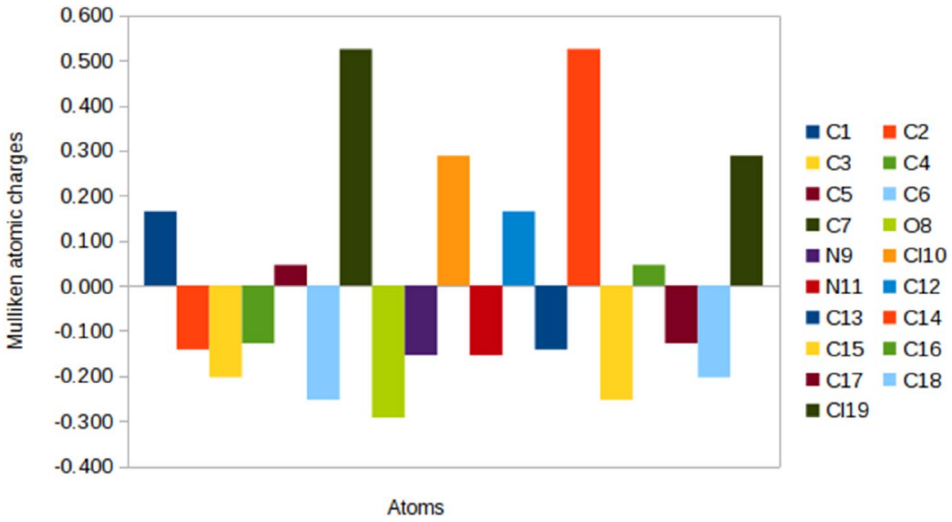

Fig. 13 Mulliken atomic charge distribution for the non-hydrogen atoms of the title compound

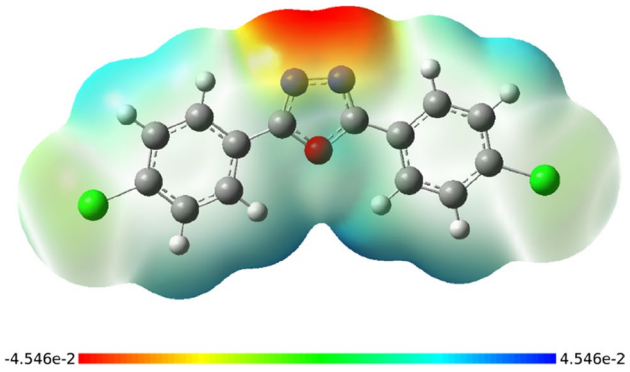

Fig. 14 Molecular electrostatic potential map of the title molecule

green color, the densities of electron in this region is low. The regions in the center of rings, such as phenyl ring and oxadiazole ring show strong steric effect as indicated by the red color.

Conclusion

Single crystal X-ray diffraction study reveals that the molecule crystallizes in the orthorhombic crystal system with the space group *Pbca*. The Hirshfeld surface analysis confirms the presence of N–H…C type intermolecular interaction. The two dimensional fingerprint plots show that the H–H contacts contribute more to the total Hirshfeld surface area (26.5%). The parameters obtained from DFT studies shows the structural parameters agree well with XRD analysis. The HOMO–LUMO energy gap of the title molecule is 4.30 eV and indicates the title molecule is stable. NCI analysis shows that the van der Waals interactions exist between chlorophenyl ring and oxadiazole ring.

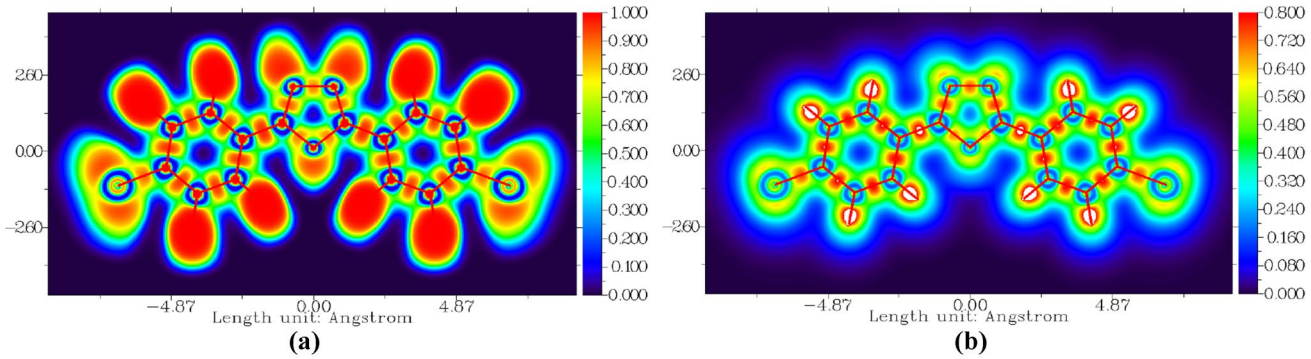

Fig. 15 ELF and LOL of the title molecule

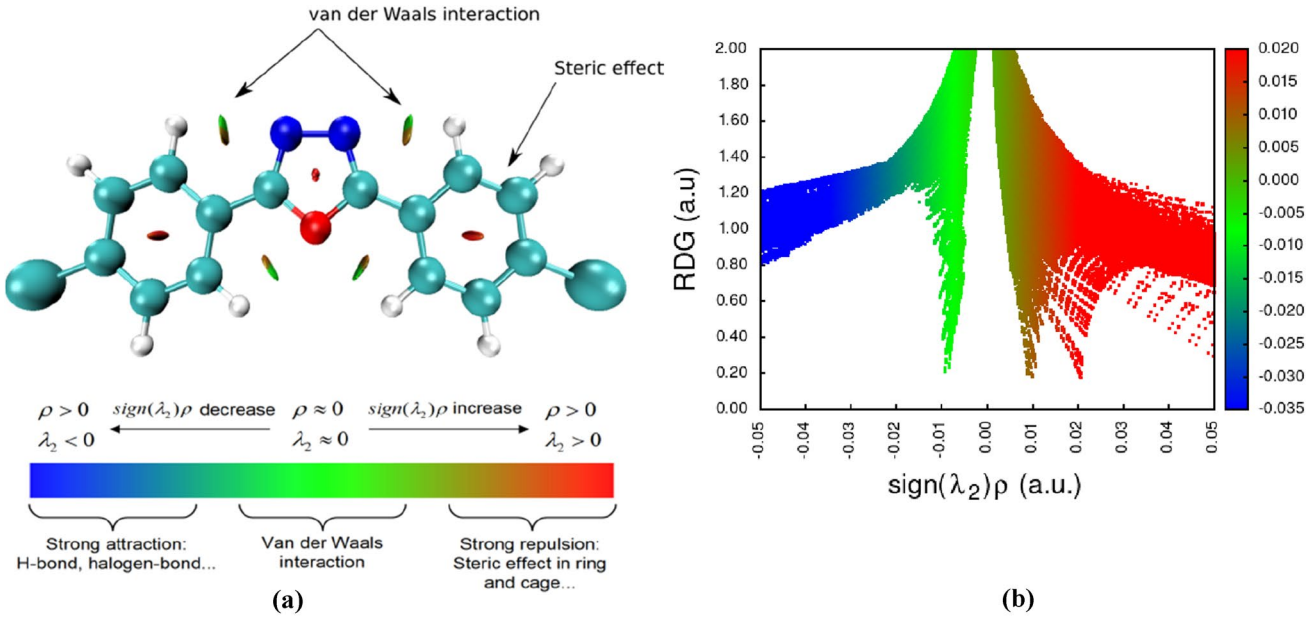

Fig. 16 The RDG isosurface and 2D scattered plot of the compound

Supporting Information

CCDC-2120182 contains the supplementary crystallographic data for this paper. These data can be obtained free of charge via https://www.ccdc.cam.ac.uk/structures/ or by e-mailing https://data_request@ccdc.cam.ac.uk or by contacting The Cambridge Crystallographic Data Centre, 12 Union Road, Cambridge CB2 1EZ, UK; fax: +44(0)1223-336033.

Acknowledgements Akhileshwari P. is thankful to DST-KSTePs, Government of Karnataka for providing the fellowship. Author thanks to SAIF for X-ray diffraction data collection.

Author Contributions PA: Conceptualization, interpretation of the data, visualization, methodology, and writing-original draft of the manuscript. KS: Synthesis and spectroscopic characterization. MAS: Investigation, supervision, and approval of the final version of the manuscript.

Data Availability The data sets generated during and/or analysed during the current study are available from the corresponding author on reasonable request.

Declarations

Conflict of interest The authors declare no conflict of interest.

References

1. Martins P, Jesus J, Santos S, Raposo LR, Roma-Rodrigues C, Baptista PV, Fernandes AR (2015) Molecules 20:16852–16891. https://doi.org/10.3390/molecules200916852
2. Henary M, Kananda C, Rotolo L, Savino B, Owens EA, Cravotto G (2020) RSC Adv 10:14170–14197. https://doi.org/10.1039/D0RA01378A
3. Lisgarten DR, Palmer RA (1998) J Chem Crys 28:725–729. https://doi.org/10.1023/A:1021856309954
4. Pearce S (2017) Drug Discov 67:137–152
5. Desai NC, Dodiya AM, Rajpara KM, Rupala YM (2014) J Saudi Chem Soc 18(3):255–261
6. Catalin VM, Fodor E, Jones PG, Daniliuc CG, Franz MH, Kelter G, Neda I (2015) Rev Roum Chim 60(1):75–83
7. Bostrom J, Hogner A, Llinas A, Wellner E, Plowright AT (2012) J Med Chem 55:1817–1830
8. Polkam N, Kummari B, Rayam P, Brahma U, Naidu VGM, Balasubramanian S, Anireddy JS (2017) ChemistrySelect 2:5492–5796
9. Kuthyala S, Shankar MK, Nagaraja GK (2018) ChemistrySelect 3(45):12894–12899
10. Rasheed H, Afridi R, Ullah A, Muhammad K, Ullah Z, Khalid S, Atiq A (2018) Inflammopharmacol 26:1037
11. He X, Li X, Liang J, Cao C, Li S, Zhang T, Meng F (2018) Bioorg Med Chem Lett 28:847
12 Lakshmithendral K, Saravanan K, Elancheran R, Archana K, Manikandan N, Arjun HA, Ramanathan M, Lokanath NK, Kabilan S (2019) Eur J Med Chem 168(1):1–10
13. Shaoyong K, Zhong L, Xuhong Q (2008) Bioorg Med Chem Lett 16(16):7565–7572. https://doi.org/10.1016/j.bmc.2008.07.026
14. Lam KW, Syahida A, Ul-Haq Z, Rahman MBA, Lajis NH (2010) Bioorg Med Chem Lett 20(12):3755–3759. https://doi.org/10.1016/j.bmcl.2010.04.067
15. Bethge K, Pertz HH, Rehse K (2005) Archiv Pharm 338:78–86
16. Yale HL, Losee K (1966) J Med Chem 9:478–483
17. Glomb T, Szymankiewicz K, Swi P (2018) Molecules 23:3361
18 Bala S, Kamboj S, Kajal A, Saini V, Nanadan Prasad D (2014). BioMed Res Int. https://doi.org/10.1155/2014/172791
19. Bentiss F, Lagrenee M, Didier B (2001) Syn Comm 31(6):935–938. https://doi.org/10.1081/SCC100103330
20 Bentiss F, Lagrenee M (1999) J Heter Chem 36(4):1029–1032. https://doi.org/10.1002/jhet.5570360433
21. Bajaj S, Kumar MS, Tinwala H, Mayur YC (2021) Bioorganic Chem 111:104873. https://doi.org/10.1016/j.bioorg.2021.104873
22. Sheldrick GM (2008) Acta Cryst A 64:112–122. https://doi.org/10.1107/S0108767307043930
23. Platon SA (1990) Acta Cryst A 46:c34. https://doi.org/10.1107/S0108767390099780
24. Macrae CF, Bruno IJ, Chisholm JA, Edgington PR, McCabe P, Pidcock E, Rodriguez-Monge L, Taylor R, van de Streek J, Wood PA (2008) J Appl Crystallogr 41:466–470. https://doi.org/10.1107/S1600576719014092
25 Allen FH, Kennard O, Watson DG, Brammer L, Orpen AG, Taylor R (1987) J Chem Soc Perkin Trans 12:S1–S19
26. Yang XJ, Drepper F, Wu B, Sun WH, Haehnel W, Janiak C (2005) Dalton Trans 2:256–267. https://doi.org/10.1039/B414999H
27. Turner MJ, McKinnon JJ, Wolff SK, Grimwood DJ, Spackman PR, Jayatilaka D, Spackman MA (2017). CrystalExplorer 175. https://doi.org/10.1107/S0108767306098199
28. Spackman MA, Jayatilaka D (2009) Cryst Eng Comm 11:19–32. https://doi.org/10.1039/B818330A
29 McKinnon JJ, Jayatilaka D, Spackman MA (2007). Chem Commun. https://doi.org/10.1039/B704980C
30. Torubaev YV, Skabitsky IV, Rozhkov AV, Galmés B, Frontera A, Kukushkin VY (2021) Inor Chem Front 8(23):4965–4975. https://doi.org/10.1039/d1qi01067k
31. Rozhkov AV, Eliseeva AA, Baykov SV, Galmes B, Frontera A, Kukushkin VY (2020) Cryst Growth Des 20(9):5908–5921. https://doi.org/10.1021/acs.cgd.0c00606
32. Gorokh ID, Adonin SA, Usoltsev AN, Novikov AS, Samsonenko DG, Zakharov SV, Fedin VP (2020) J Mol Struct 1199:126955. https://doi.org/10.1016/j.molstruc.2019.126955
33. Adonin SA, Gorokh ID, Novikov AS, Samsonenko DG, Korolkov IV, Sokolov MN, Fedin VP (2017). Polyhedron. https://doi.org/10.1016/j.poly.2017.11.002
34. Adonin SA, Gorokh ID, Samsonenko DG, Novikov AS, Korolkov IV, Plyusnin PE, Fedin VP (2019) Polyhedron 159:318–322. https://doi.org/10.1016/j.poly.2018.12.017
35. Mahmoudi G, Seth SK, Bauza A, Zubkov FI, Gurbanov AV, White J, Frontera A (2018) CrystEngComm 20(20):2812–2821. https://doi.org/10.1039/c8ce00110c
36. Adonin SA, Gorokh ID, Novikov AS, Usoltsev AN, Sokolov MN, Fedin VP (2019) Inorg Chem Commun 103:72–74. https://doi.org/10.1016/j.inoche.2019.03.014
37. Spackman MA, McKinnon JJ (2002) Cryst Eng Comm 4(66):378–392. https://doi.org/10.1039/B203191B
38. Mackenzie CF, Spackman PR, Jayatilaka D, Spackman MA (2017) IUCrJ 4:575–587
39. Turner MJ, Thomas SP, Shi MW, Jayatilaka D, Spackman MA (2015) Chem Comm 51:3735–3738
40. Frisch MJ, Trucks GW, Schlegel HB, Scuseria GE, Robb MA, Cheese-man JR, Scalmani G, Barone V, Petersson GA, Nakatsuji H, Li X, Caricato M, Marenich A, Bloino J, Janesko BG, Gomperts R, Mennucci B, Hratchian HP, Ortiz JV, Izmaylov AF, Sonnenberg JL, Williams-Young D, Ding F, Lipparini F, Egidi F, Goings J, Peng B, Petrone A, Henderson T, Ranasinghe D, Zakrzewski VG, Gao J, Rega N, Zheng G, Liang W, Hada M, Ehara M, Toyota K, Fukuda R, Hasegawa J, Ishida M, Nakajima T, Honda Y, Kitao O, Nakai H, Vreven T, Throssell K, Montgomery JA Jr, Peralta JE, Ogliaro F, Bearpark M, Heyd JJ, Brothers E, Kudin KN, Staroverov VN, Keith T, Kobayashi R, Normand J, Raghavachari K, Rendell A, Burant JC, Iyengar SS, Tomasi J, Cossi M, Millam JM, Klene M, Adamo C, Cammi R, Ochterski JW, Martin RL, Morokuma K, Farkas O, Foresman JB, Fox DJ (2009) Gaussian 09. Gaussian Inc, Wallingford CT
41. Mary YS, Miniyar PB, Mary YS, Resmi KS, Panicker CY, Armaković S, Armaković SJ, Thomas R, Sureshkumar B (2018). J Mol Struct. https://doi.org/10.1016/j.molstruc.2018.07.026
42. Chortani S, Edziri H, Manachou M, Al-Ghamdi YO, Almalkie SG, Alqurashi YE, Ben Jannet H, Romdhane A (2020) J Mol Struct 1217:128357
43. Pearson RG (2005) J Chem Sci 117(5):369–377
44. Zhou JH, Zheng LW, Yan MC, Shi MJ, Liu J, Shangguan GQ (2017). J Chem. https://doi.org/10.1155/2017/6537402
45. Gasteiger J, Li X, Rudolph C, Sadowski J, Zupan J (1994) J Amer Chem Soc 116:4608–4620
46. Savin A, Nesper R, Wengert S, Fassler TF (1997) Angew Chem Int Ed Engl 36:1808–1832
47 Seema SK, Vinay SK, Chidanandayya S, Sudhir Hiremath M, Mahantesha B, Radder SB (2019) J Mol Struct 1196:280–290. https://doi.org/10.1016/j.molstruc.2019.06.078
48. Humphrey W, Dalke A, Schulten KJ (1996) J Mol Graph 14(1):33–38. https://doi.org/10.1016/0263-7855(96)00018-5
49. Lu T, Chen F (2012) J Comput Chem 33:580–592. https://doi.org/10.1002/jcc.22885
50. Laplaza R, Peccati FA, Boto R, Quan C, Carbone A, Piquemal J, Maday Y, Garcia JC (2020) J WIREs Comput Mol Sci 1497:1–18. https://doi.org/10.1002/wcms.1497

Authors and Affiliations

P. Akhileshwari[1] · K. Sharanya[2] · M. A. Sridhar[1]

[1] Department of Studies in Physics, Manasagangotri, University of Mysore, Mysuru 570006, India

[2] PG Department of Chemistry, Sri Dharmasthala Manjunatheshwara College (Autonomous), Ujire, Karnataka 574240, India